"Large Scale Accelerator Production of ^{225}Ac: Effective Cross Sections for 78-192 MeV Protons Incident on ^{232}Th Targets"*

J. R. Griswold[a,b,†], D. G. Medvedev[c], J. W. Engle[d], R. Copping[a], J. M. Fitzsimmons[c], V. Radchenko[d], J. C. Cooley[d], M. E. Fassbender[d], D. L. Denton[a], K. E. Murphy[a], A. C. Owens[a], E. R. Birnbaum[d], K. D. John[d], F. M. Nortier[d], D. W. Stracener[e], L. H. Heilbronn[b], L. F. Mausner[c], S. Mirzadeh[a]

[a]Nuclear Security and Isotope Technology Division, Oak Ridge National Laboratory, Oak Ridge, TN 37831

[b]Department of Nuclear Engineering, University of Tennessee, Knoxville, TN 37996

[c]Collider-Accelerator Department, Brookhaven National Laboratory, Upton, NY 11973

[d]Los Alamos National Laboratory, Los Alamos, NM 87545

[e]Physics Division, Oak Ridge National Laboratory, Oak Ridge, TN 37831

Abstract

Actinium-225 and ^{213}Bi have been used successfully in targeted alpha therapy (TAT) in preclinical and clinical research. This paper is a continuation of research activities aiming to expand the availability of ^{225}Ac. The high-energy proton spallation reaction on natural thorium metal targets has been utilized to produce millicurie quantities of ^{225}Ac. The results of sixteen irradiation experiments of thorium metal at beam energies between 78 and 192 MeV are summarized in this work. Irradiations have been conducted at Brookhaven National Laboratory (BNL) and Los Alamos National Laboratory (LANL), while target dissolution and processing was carried out at Oak Ridge National Laboratory (ORNL). Excitation functions for actinium and thorium isotopes, as well as for some of the fission products, are presented. The cross

† This work constitutes a portion of JRG's thesis for the Doctor of Philosophy Degree at the University of Tennessee.

sections for production of ^{225}Ac range from 3.6 to 16.7 mb in the incident proton energy range of 78 to 192 MeV. Based on these data, production of curie quantities of ^{225}Ac is possible by irradiating a 5.0 g cm^{-2} ^{232}Th target for 10 days in either BNL or LANL proton irradiation facilities.

Keywords: ^{225}Ac, ^{226}Ac, ^{227}Ac, ^{227}Th, ^{228}Th, ^{99}Mo, ^{140}Ba, ^{139}Ce, ^{141}Ce, ^{143}Ce, ^{144}Ce, Actinium, Alpha-emitting, Radiotherapy, Proton irradiation, Thorium

1. Introduction

The scientific community has produced many new diagnostic and therapeutic applications for the field of nuclear medicine over the last few decades. One of these therapeutic applications, targeted alpha radioimmunotherapy (also referred to targeted alpha therapy or TAT), is one of the most promising and effective new methods of treating various forms of oncologic diseases (Essler et al., 2012). This technique involves delivering selected alpha-emitting radionuclides to cancerous sites within the body. Among possible α-emitting radionuclides, currently there is a great interest in the use and application of ^{213}Bi. Results of clinical trials with ^{213}Bi (in the decay chain of ^{225}Ac) eluted from a generator have shown progress in treating several different types of malignant diseases including acute myeloid leukemia (Jurcic and Rosenblat, 2014).

In addition to the generator mode, there have been some investigations focusing on the direct *in vivo* administration of ^{225}Ac (McDevitt et al., 2001). The four α-particle emission decay chain of ^{225}Ac results in an integrated dose that is about 1000 times larger than the dose from an equivalent quantity of ^{213}Bi, which only decays with the emission of a single α-particle (Mirzadeh, 1998; Brechbiel, 2007). Despite the potential complications associated with the decay products leaving the tumor volume and damaging healthy tissue, this mode of therapy utilizing ^{225}Ac remains attractive due to its potency. Hence, there is a continuous effort to develop approaches designed to overcome this issue (McLaughlin et al., 2013; Mulvey et al., 2013; Rojas et al., 2015), and a recent review is available (de Kruijff et al., 2015). Whether used via the direct application or as a generator for ^{213}Bi, the efficacy in early clinical trials has greatly increased the demand for ^{225}Ac.

Currently, the only method of generating ^{225}Ac for clinical studies is through the decay of long-lived ^{229}Th ($t_{1/2}$ = 7880 y) (Boll et al., 2005). Using this technique, ^{225}Ac and its direct

parent ^{225}Ra ($t_{1/2}$ = 14.9 d) are routinely "milked" from the "cow" (^{229}Th) every few weeks. At present, there are three main sources of ^{229}Th worldwide that are large enough to produce relevant quantities of ^{225}Ac. Each of these sources has been chemically separated from the fissile precursor ^{233}U (Figure S1). Since 1997, ORNL has been supplying up to 720 mCi per year of high-purity ^{225}Ac. A similar quantity is reported to be available from the Institute of Physics and Power Engineering, in Obninsk, Russia. The Institute for Transuranium Elements in Karlsruhe, Germany (ITU) maintains a smaller ^{229}Th source that is capable of producing up to 350 mCi of ^{225}Ac per year (IAEA, 2013). Demand, even to support a few limited clinical trials, is much larger than the combined international inventory.

Studies have been conducted to investigate different means of increasing the available supply of either the ^{229}Th parent or ^{225}Ac itself. Producing relevant quantities of ^{229}Th is challenging due to its extremely long half-life. Despite the ~160 mb cross section for the ^{232}Th[p,4n]^{229}Pa reaction at ~30 MeV, dedicated accelerator production of ^{229}Th may not be viable due to long irradiation times and high currents required to produce a substantial quantity of ^{229}Th (Jost et al., 2013). However, substantial ^{229}Th could be generated if ^{232}Th were used as a beam stop for several years at any high-current proton accelerator facility. Reactor production of ^{229}Th is possible through the neutron irradiation of ^{226}Ra ($t_{1/2}$ = 1600 y) and is currently under further investigation (Boll et al., 2008). Proton irradiation of ^{226}Ra targets has been carried out at ITU resulting in cross section data for the ^{226}Ra[p,2n]^{225}Ac reaction for the energy range of 8.8 to 24.8 MeV, with a maximum cross section of 710 mb at 16.8 MeV (Apostolidis et al., 2005). A feasibility study of the ^{226}Ra[γ,n]^{225}Ra reaction for producing the ^{225}Ra, the parent to ^{225}Ac, has revealed that ^{225}Ra yields are insufficient for practical use (Melville et al., 2007).

Actinium-225 can be directly generated through the high-energy proton (78-192 MeV) irradiation of ^{232}Th (Lefort et al., 1961; Gauvin, 1963; Titarenko et al., 2003; Ermolaev et al., 2012; Weidner et al., 2012). The U.S. Department of Energy (DOE) Isotope Program operates two high-current, high-energy linear accelerators capable of producing ^{225}Ac from ^{232}Th in substantial quantities. The primary focus of this study is the practical evaluation of the feasibility of producing ^{225}Ac using DOE operated facilities, and preliminary results are reported in a previous document (Mirzadeh, 2014). The Brookhaven Linac Isotope Producer (BLIP) at BNL, the Isotope Production Facility (IPF) at LANL, and the Medical Radioisotope Program (MRP) at ORNL engaged in distinct and critical roles for this project. IPF and BLIP were responsible for

the irradiation of the Th targets, and MRP performed the chemical separations required to isolate ^{225}Ac.

In this paper, we report effective cross section and yield measurement for large-scale production of ^{225}Ac. We also report cross sections for several other radioisotopes including: ^{226}Ac, ^{227}Ac, ^{227}Th, ^{228}Th, ^{99}Mo, ^{140}Ba, ^{139}Ce, ^{141}Ce, ^{143}Ce, and ^{144}Ce. Measurement of yield of the other actinium isotopes relative to ^{225}Ac is crucial since the coproduced actinium isotopes cannot be chemically separated and, hence, they constitute major impurities. The effective cross sections[*1] and yields of the other radioisotopes are included due to their effect on chemical processing and purity of the ^{225}Ac product, among the most important are isotopes of La (^{140}Ba decays to ^{140}La) and Ce due to their very close chemical resemblance to Ac. The details of the chemical isolation of actinium from fission products and actinides coproduced in the high-energy proton irradiation of natural Th is beyond the scope of this current paper, and it will be reported separately.

2. Materials and Methods

2.1 Irradiation Facilities

The irradiation facilities used in this work differ from each other in proton intensity and energy capabilities. The BNL Linac is capable of generating 130 μA of protons up to 200 MeV for use in the BLIP beam line and target area (Raparia et al., 2014). As part of the LANSCE accelerator system at LANL, IPF is a dedicated proton beam line that can provide up to 250 μA of 100 MeV protons (Lisowski and Schoenberg, 2006).

2.2 Irradiations

A total of sixteen irradiations were performed, three at IPF and thirteen at BLIP. Irradiation parameters such as incident proton energy, irradiation period, and target thickness were adjusted to meet the specific goals of each experiment. The parameters for each irradiation at BLIP and

[1] The term "effective cross section" is used to reflect that there may be a number of nuclear pathways to a specific radionuclide and to reflect that the targets used in our studies are not considered "thin" targets. Consequently, some loss of proton energy occurred in each target. General notation of type ^{232}Th[p,x]^{225}Ac was used to highlight the multiple reaction pathways; in this specific case, ^{232}Th[p,α4n]^{225}Ac and ^{232}Th[p,αp3n]^{225}Ra(β-, 14.9 d)→^{225}Ac. From this point forward, the term "cross section" refers to the "effective cross section."

LANL are summarized in Table 1. Overnight irradiations were designed to measure cross sections for the short-lived impurities such as ^{226}Ac ($t_{1/2}$ = 29.37 h) and ^{143}Ce ($t_{1/2}$ = 33.04 h). Longer irradiations were carried out to achieve three primary objectives: (a) to produce useful quantities of ^{225}Ac for evaluation in nuclear medicine applications, (b) to develop the remote chemical process adaptable to large-scale production of ^{225}Ac, and (c) to resolve the often challenging logistical issues associated with the shipment of highly radioactive targets containing alpha emitting radionuclides.

2.2.1 Irradiations at LANL-IPF

At LANL, Th metal was arc-melted and rolled to the thickness of the finished target, and then it was trimmed to its final dimensions. X-ray Fluorescence Spectroscopy of Th stock confirmed a composition ≥ 99.6%. These Th discs were electron-beam welded into machined Inconel capsules (Figure S2). During irradiations at IPF, instantaneous beam intensities were monitored and logged at one and ten second intervals by two inductive current monitors. Log files were reconstructed into beam histories, with radionuclide production and decay in each time step accounted for in yield calculations described below. In the past, recorded beam histories have been compared with integrated fluences measured by established monitor reactions (Weidner et al., 2012) and found to be accurate within 5%.

After irradiation, targets were allowed to decay at IPF to U.S. Department of Transportation (DOT) Type A quantities and then moved to the processing facility where the Inconel encapsulation was cut open. The irradiated Th was then removed from the Inconel cladding, repackaged in a glass vial, and shipped to ORNL for chemical processing.

2.2.2 Irradiations at BNL-BLIP

For the irradiations at BLIP, Th foils (0.125 mm, 99.5% purity) were purchased from Goodfellow Corporation (Coraopolis, Penn., USA). For a typical irradiation, a ~27.9 mm circle was cut from the foil and wrapped in 0.025 mm Al metal foil to prevent contamination spread during target opening and packaging for shipment. A single foil was irradiated in the shorter irradiations while three sandwiched foils were irradiated in the longer ones. The beam current was monitored using 0.127 mm Al foil (99.99%, Atlantic Metals and Alloys, LLC) whose area mimicked that of the Th foils. Since BLIP targets are cooled by water, in all experiments the foils and Al monitor foil were isolated in a bolted aluminum target capsule described previously

(Medvedev et al., 2012). The well of the target capsule was machined to the size of the Th and Al foil stack to ensure close fit for good thermal conductivity (Figure S3). After irradiation, the aluminum monitor foil was dissolved in a mixture of HCl and HNO_3, and the resulting solution was assayed for ^{22}Na ($t_{1/2}$ = 2.6 y) using γ-ray spectroscopy. Resulting beam current was determined from the activation equation (Helus and Wobler, 1983) using cross section data from Steyn et al. (Steyn et al., 1990).

Before shipment of the more radioactive targets, each target was allowed to decay for seven days to reduce the dose and radioimpurities to levels that met transportation and radiological facility requirements. The foils were packaged and shipped individually in DOT Type A containers.

2.3 Target Dissolution and Processing at ORNL

After arrival at ORNL, the targets were transferred into a hot cell for remote processing, as the radiation dose measured on contact with the target foils was usually greater than 60 mSv/h. Each foil was dissolved in 10 M optima grade HCl with a few drops of 2 M HF. Gentle heating was applied to aid the dissolution. After dissolution, the supernatant solution was separated from residual solids by decantation, and a 50 µL aliquot was taken from each dissolved sample and diluted to 5–10 × 10^4 times to reduce the sample activity enough for γ-ray spectroscopy analysis. Activities of all radioisotopes reported in this work except for ^{227}Ac ($t_{1/2}$ = 21.77 y) were determined from this target solution aliquot.

Since ^{227}Ac does not emit abundant γ-rays, its activity was determined by measuring the activity of its daughter, ^{227}Th, after it reached secular equilibrium with ^{227}Ac. Two approaches were used: In the first approach, an aliquot of target solution was allowed to decay for at least180 days and then it was assayed for ^{227}Th. The second approach was used in later experiments as it facilitated faster results; the Ac fraction was chemically separated from Th and ^{227}Th was then allowed to grow in the purified ^{227}Ac fraction. The resulting ^{227}Ac activity was corrected taking into account chemical yield of the actinium fraction which was monitored through the detection of ^{225}Ac.

Ion exchange and extraction chromatography were used to separate actinium from the Th target, isotopes of Pa and Ra, and the large number of fission products generated in each

irradiation. Although a detailed explanation of the chemical purification is beyond the scope of this manuscript, a brief description is useful to outline the measures required to determine the chemical yield of actinium, specifically ^{227}Ac.

Chemical processing varied slightly for each target, as new methods and process optimization were implemented after each irradiation. The most commonly used procedure employed a series of anion exchange columns for bulk Th removal (Boll et al., 2005) followed by a lanthanide/actinium separation. Typically, chemical processing consisted of five ion exchange columns. Briefly, the first anion exchange column was used in 10 M HCl media to facilitate separation of Ac from Pa isotopes and most of the higher activity non-lanthanide fission products, such as Mo and Ag. The second and third anion exchange columns used 8 M HNO_3 media to separate the large quantity of Th still present in the dissolved target solution. Next, a cation exchange column was used to separate the divalent alkali earth metals (Ca, Sr, Ba, and Ra) from the Ac (1.2 M HNO_3) and also to eliminate trace amounts of Ag that leaked from the first column. This was followed by an actinium/lanthanide separation column using extraction chromatography, such as Eichrom Ln resin (Mirzadeh, 2014) or DGA resin (Radchenko et al., 2015). This aspect of the separation is highly sensitive as the lanthanide (III) and actinium (III) cations exhibit very similar chemical properties. All fractions of each ion exchange column were collected for analysis and diluted as necessary for γ-ray spectroscopy.

2.4 Gamma-Ray Spectroscopy

The radioactivity measurements were conducted using a well-shielded, Canberra Model GC2020 High-Purity Germanium detector with a relative efficiency of 20%. A PC-based multichannel analyzer utilizing Canberra Genie 2000 software was coupled to the detector. The measured resolution of the detector was 2.0 keV at 1.33 MeV. Energy and efficiency calibrations were completed using a γ-ray source traceable to the National Institute of Standards and Technology (NIST). Spectra collection times varied from one-hour counts for initial sample dilutions to 36-hour counts for severely decayed samples. Sample to detector geometry was varied to reduce the detector dead time below 5%. Each peak in the γ-ray spectra was fitted using the non-linear least squares fit method (Canberra, 2009). When possible, multiple γ-ray peaks were used to quantify the activity at end of bombardment (EOB) for each radioisotope through a weighted average method. Often, only two γ-rays from each radionuclide were used due to the

complicated spectrum generated from hundreds of fission products and a number of isotopes of Pa, Th, Ac, Ra, and several decay daughters of these chains. Two examples of spectra collected over the course of this project are shown below. The top half of Figure 1 shows a γ-ray spectrum of a dissolved foil sample within one day of dissolution and within three days of EOB, and the bottom half of Figure 1 shows the same sample spectrum after ~16 months of decay.

The principal γ-ray energies, intensities, and appropriate branching ratios (if necessary) used in this study (Table 2) were acquired from the Nuclear Data Sheets (Artna-Cohen, 1997; Browne, 2001; Burrows, 2001; Sonzogni, 2001; Browne, 2005; Basunia, 2007; Kumar Jain et al., 2007; Nica, 2007; Browne and Tuli, 2011; Singh et al., 2011; Browne and Tuli, 2012; Nica, 2014).

Resulting activities were corrected back to EOB, and cross sections were calculated by using the activation equation $\sigma_{eff} = \frac{A}{N \cdot \bar{I}_p}(1 - e^{-\lambda_i t_{irr}})^{-1}$, where, σ_{eff} is effective cross section, A is radioactivity (dps), N is target surface density (atoms.cm^{-2}), $\bar{I}_p$ is average proton intensity (protons per sec), λ_i is the decay constant of the radioisotope of interest (s^{-1}), and t_{irr} is irradiation time (s). Appropriate corrections were also applied for radioactive decay during counting using the equation $A = \frac{\lambda_i C}{(1-e^{-\lambda_i t})\varepsilon I_\gamma}$ where A is radioactivity, C is the uncorrected count rate, t is the count time, ε is the energy-dependent detector efficiency, and I_γ is the γ-ray intensity. Cross section uncertainties were calculated using error propagation with estimated uncertainties for target mass (6.7–11.9%), beam intensity (7–10%), and sampling and detector efficiency (5%).

3. Results

Cross sections of the isotopes of interest are given in Tables 3–4 and depicted in Figures 2–5. Measured cross sections at 89.6, 128.0, and 191.8 MeV are given as averages with propagated uncertainty since two irradiations at IPF occurred at 89.6 MeV, six irradiations at BLIP occurred at 128.0 MeV, and five additional irradiations at BLIP occurred at 191.8 MeV. Note that the incident proton energy at 191.8 MeV ranges from 190.9 MeV to 192.5 MeV (Table 1). As shown in Figures 2–5, the cross sections measured in this work mimic the energy dependence shown by cross sections reported previously (Lefort et al., 1961; Gauvin, 1963; Holub and Yaffe, 1973;

Hogan et al., 1979; Duijvestijn et al., 1999; Titarenko et al., 2003; Ermolaev et al., 2012; Weidner et al., 2012; Engle et al., 2014).

The cross sections for the ^{232}Th[p,x]^{225}Ac reaction in the 20–200 MeV energy range are plotted together with literature values in Figure 2. As seen, cross sections for ^{225}Ac increase rather linearly from 3.6 ± 0.5 mb at E_p = 77.8 MeV to 16.7 ± 1.6 mb at E_p = 170.7 MeV and then decrease to 14.0 ± 1.6 mb at 191.8 MeV (Figure 2 and Tables 3–4). Cross sections measured for the ^{232}Th[p,x]^{226}Ac reaction in the 128–200 MeV incident proton energy range together with literature values (E_p = 20–200 MeV) are shown in Figure 2. Cross sections for this reaction also increase linearly from 8.1 ± 1.0 mb to 14.7 ± 1.7 mb at energies of 128.0 to 191.8 MeV, respectively. As with the other isotopes of Ac, the cross sections for the ^{232}Th[p,x]^{227}Ac reaction increases from 4.5 ± 0.7 mb at 77.8 MeV to 6.3 ± 1.0 mb at 89.6 MeV (Figure 2). At 128.0 MeV, the cross section increases to 26.5 ± 3.5 mb, which differs by as much as a factor of three from literature values. This may be due to complexities in the quantification of the long-lived ^{227}Ac radionuclide, which are covered in the Discussion section.

Although several other isotopes of Th are generated in these irradiations, only the cross sections for the ^{232}Th[p,x]^{227}Th and ^{232}Th[p,x]^{228}Th reactions are presented here in Figure 3. For the ^{232}Th[p,x]^{227}Th reaction, cross sections exhibit a maximum of 37.2 ± 5.0 mb at 77.8 MeV followed by a slight decrease to a minimum value of 24.3 ± 2.7 mb at 170.7 MeV. Similarly, the cross section for the ^{232}Th[p,x]^{228}Th reaction decreases from 56.7 ± 7.2 mb to 37.1 ± 3.1 mb at 77.8 and 191.8 MeV respectively.

Cross sections and the relevant literature comparisons are shown in Figures 4–5 for proton-induced fission of Th. A few examples of these reactions include: ^{232}Th[p,f]^{99}Mo, ^{232}Th[p,f]^{140}Ba, and ^{232}Th[p,f]^{139,141,143,144}Ce reactions. The excitation function for ^{99}Mo remains relatively constant and varies only within uncertainty limits ranging from 36.3 ± 3.4 mb to 25.8 ± 3.4 mb (Figure 4). The cross sections for the ^{232}Th[p,f]^{140}Ba reaction decrease continuously from a maximum value of 14.2 ± 1.8 mb at E_p = 77.8 MeV to 5.2 ± 1.1 mb at E_p = 191.8 MeV (Figure 4). With the exception of the ^{232}Th[p,f]^{139}Ce reaction, the cross sections for all of the reported ^{232}Th[p,f]Ce reactions decrease almost linearly with increasing incident proton energy (Figure 5). Note that the measurement of the cross section for the ^{232}Th[p,f]^{139}Ce reaction at 128.0 MeV is approximately a factor of two higher than the literature values.

4. Discussion

4.1 ^{232}Th[p,x]Ac reactions

The data for the ^{232}Th[p,x]^{225}Ac reaction is in close agreement with literature values at E_p < 170 MeV but ~25% lower than literature values at E_p = 191.8 MeV (Figure 2). Note that the cross section for this reaction includes a contribution from the β^- decay of ^{225}Ra, as well as a contribution from the electron capture decay (~10%) of ^{225}Th ($t_{1/2}$ = 8.75 m). Earlier measurements showed that the cross section for the ^{232}Th[p,x]^{225}Ra reaction over this energy range is smaller than the ^{232}Th[p,x]^{225}Ac cross section by a factor of 5–10 (Zhuikov et al., 2011; Weidner et al., 2012); therefore, contribution from ^{225}Ra decay will not be significant. However, efforts are in progress to quantify the ^{225}Ra yield for this set of experiments, as the ^{232}Th[p,x]^{225}Ra(β^-)^{225}Ac route will provide ^{225}Ac free from ^{227}Ac contamination. Presently, the effect of ^{227}Ac contamination on the performance of the ^{225}Ac/^{213}Bi generator and its effect on *in vivo* toxicity of accelerator produced ^{225}Ac are unknown but studies are currently under way to determine its effect.

The relatively short half-life of ^{226}Ac (29.4 h) limits the detection of this radionuclide because of the long delay between the end of bombardment and target assay. However, measurement of the production cross section of ^{226}Ac was possible in the overnight irradiations at BLIP followed by next day shipment. This enabled target assay approximately three days after EOB. The cross section values presented here are slightly lower than the previous measurements by Lefort *et al.* (Lefort et al., 1961) and Engle *et al.* (Engle et al., 2014). Actinium-226 is also fed through α-decay of ^{230}Pa, produced via the ^{232}Th[p,3n] reaction. No decay contributions were considered for this reaction since the α-branching ratio of ^{230}Pa is < 0.1%.

In addition to direct formation, ^{227}Ac activity is fed by the decays of ^{227}Ra ($t_{1/2}$ = 42.2 m) and ^{231}Pa ($t_{1/2}$ = 32,760 y), but this effect is insignificant. The cross section for ^{227}Ra is likely much lower than for ^{227}Ac due to the ejection of an additional proton. At the same time, α-decay of ^{231}Pa has a negligible effect on the cumulative cross section because of its long half-life. As pointed out earlier, an accurate quantification of ^{227}Ac required chemical isolation of the actinium fraction. The weak γ-ray emissions of ^{227}Ac combined with the complex γ-ray spectra associated with the irradiated Th foils caused the direct measurement of this long-lived radioisotope to be challenging. However, the activity of the daughter nuclei of ^{227}Ac, ^{227}Th

($t_{1/2}$ = 18.72 d), was determined through the detection of the 236 keV (12.9%) γ-ray, and in a few instances it was possible to re-assay a sample of the target solution (dissolved foil) 12 to 18 months post EOB. This allowed ^{227}Th to reach secular equilibrium with ^{227}Ac while directly produced ^{227}Th decayed below the limit of detection. Further, decay of a number of longer lived fission products such as ^{103}Ru ($t_{1/2}$ = 39.2 d) and ^{95}Zr ($t_{1/2}$ = 64.0 d) during this period resulted in a net reduction of the overall Compton continuum and hence an improvement in detection sensitivity. This is clearly demonstrated in the examples of spectra shown in Figure 1.

In the case of the later irradiations, ^{227}Ac activity was derived from the purified Ac fraction. After chemical separation, an aliquot of the Ac fraction was assayed by γ-ray spectroscopy to determine the activity of ^{227}Ac and ^{227}Th. Comparison of ^{225}Ac activity values in the target solution and in the Ac fraction provided an overall chemical yield. Thorium-227 was then allowed to grow into full secular equilibrium in the above sample (for >180 days) and then re-assayed, providing an accurate measure of the ^{227}Ac which was then corrected taking into account chemical yield. The cross sections for the ^{232}Th[p,x]^{227}Ac reaction measured in this work agree with literature values with the exception of the data point at 128.0 MeV. At this energy, previous literature measurements are lower by a factor >2. The source of this discrepancy is currently unknown.

4.2 ^{232}Th[p,x]Th reactions

Of the other Th isotopes produced in these experiments but not reported here, only ^{231}Th is realistically detectable via γ-ray spectroscopy. Unfortunately, the principal γ-ray emission for ^{231}Th is a low-energy, low-intensity photon in the X-ray region (84.2 keV, 6.6%). Because of the complex γ-ray spectra generated by the irradiated foil, distinguishing this emission from background was not possible. Very small quantities of ^{229}Th ($t_{1/2}$ = 7932 y) and ^{230}Th ($t_{1/2}$ = 75,400 y) are also likely generated in these irradiations, but their long half-lives and hence small irradiation yields make quantification by γ-ray spectroscopy impractical.

Cross sections measured here for the ^{232}Th[p,x]^{227}Th reaction agree with the data reported by Lefort *et al.* (Lefort et al., 1961) and Hogan *et al.* (Hogan et al., 1979) at lower energies (below 100 MeV, Figure 3). Weidner *et al.* (Weidner et al., 2012) reported a slightly higher value at the lower energies, while Ermolaev *et al.* (Ermolaev et al., 2012) reported a marginally lower value. Similar to the cross sections reported in this work, it is important to note that the cross sections

reported by Ermolaev *et al.* (Ermolaev et al., 2012) do not represent "thin target" cross sections as the target thickness was ~50 mg cm^{-2} in this experiment. Cross sections reported here are slightly lower than literature values in the 125 to 180 MeV range. The contribution of ^{227}Ac decay to the cumulative cross section of ^{227}Th in the reaction is negligible due to the substantial difference in half-lives of these radionuclei. However, the decay of ^{227}Pa (EC = 15%, $t_{1/2}$ = 38.3 m) does add to the cumulative cross section.

As shown in Figure 3, data sets of previous cross section measurements for the ^{232}Th[p,x]^{228}Th reaction in the displayed energy range vary substantially — especially in the energy range of this work (70 to 200 MeV). Similar to the quantification of ^{227}Ac, ^{228}Th required a cool-off period to be accurately quantified in the target solution. Thorium-228 emits only weak γ-rays; therefore, the daughter products ^{224}Ra ($t_{1/2}$ = 3.63 d) and ^{212}Pb ($t_{1/2}$ = 10.6 h) must be utilized to accurately measure the activity of ^{228}Th. Since some ^{224}Ra was generated directly in the target, a sample of the target solution was allowed to decay for >30 days post EOB before assay for ^{224}Ra/^{212}Bi activity. In practice, the decay period was often longer than 30 days to facilitate the detection of other long-lived isotopes such as ^{227}Ac and ^{144}Ce ($t_{1/2}$ = 285.0 d). The cross sections measured in this work for the ^{232}Th[p,x]^{228}Th reaction are in good agreement with the literature values (Figure 3). This cumulative reaction cross section includes significant contributions from the decays of ^{228}Pa (EC = 98.15%, $t_{1/2}$ = 22.4 h) and ^{228}Ac (β^- = 98.15%, $t_{1/2}$ = 6.15 h). A comparison of the cross-sections of ^{232}Th[p,x]^{228}Th and ^{232}Th[p,x]^{227}Th reactions (Figure 3), clearly indicates the effect of ejecting one additional nucleon from the target nucleus as the threshold energy for the ^{232}Th[p,x]^{228}Th reaction is ~10 MeV lower than the threshold for the ^{232}Th[p,x]^{227}Th reaction. Further, the magnitude of the cross section for the ^{232}Th[p,x]^{228}Th reaction is higher by about a factor of two. This effect is not, however, apparent for the series of ^{232}Th[p,x]^{225,226,227}Ac reactions (Figure 2).

4.3 Selected Fission Products: ^{232}Th[p,f]^{99}Mo, ^{140}Ba, and ^{139,141,143,144}Ce reactions

The cross sections for the ^{232}Th[p,f]^{99}Mo reaction ranging from 25.8 to 36.3 mb in the 75 to 92 and 120 to 180 MeV energy range are reported for the first time (Figure 4). Cross sections for this reaction are relatively constant and exhibit only small variations over the incident proton energy range. Previously reported reaction cross sections for the ^{232}Th[p,f]^{140}Ba reaction are in excellent agreement with the cross sections reported here (Figure 4) (Holub and Yaffe, 1973;

Duijvestijn et al., 1999; Titarenko et al., 2003; Engle et al., 2014). As with the other long-lived nuclides mentioned previously, several of the cerium isotopes required a cool-off period for the background to subside so that the photopeaks could be measured accurately. Cerium-139 ($t_{1/2}$ = 137.6 d), ^{141}Ce ($t_{1/2}$ = 32.5 d), and ^{144}Ce were assayed in the target solution at least 90 days post EOB. When comparing with the results from Engle *et al.* (Engle et al., 2014), the cross sections measured in this work for the ^{232}Th[p,f]^{139}Ce reaction are in good agreement except for measurements at 128.0 MeV, where the results differ by a factor >2 (Figure 5). Again, this large discrepancy is likely due to the difficulty in measuring long-lived radioisotopes in the presence of many short-lived radionuclides via γ-ray spectroscopy. Cross sections for the ^{232}Th[p,f]^{141}Ce reaction are generally lower than the most recent published values (Titarenko et al., 2003; Engle et al., 2014) (Figure 5). The values reported here for the ^{232}Th[p,f]^{143}Ce and ^{232}Th[p,f]^{144}Ce reactions also agree consistently with the literature data, except in the case of the 128.0 MeV cross section of ^{143}Ce where the data reported here are lower by a factor >2 than the measured cross section reported earlier (Engle et al., 2014) (Figure 5). As indicated, while cross sections for ^{232}Th[p,f]$^{141, 143, 144}$Ce reactions decrease with increasing incident proton energy, the cross section for ^{232}Th[p,f]^{139}Ce reaction increases with incident proton energy. An explanation for this may relate to the fact that ^{141}Ce, ^{143}Ce, and ^{144}Ce are neutron-rich nuclei, decaying with β^- emission, while ^{139}Ce is proton-rich and decays via electron capture.

A comprehensive review of data related to fission of Th targets in these experiments is beyond the scope of the present work. However, in low to moderate proton energies, the yields of specific products are expected to show yield-versus-mass curves that are rather flat on the top, but have more defined peaks at slightly lower than half the mass of Th (A = 232) (Hudis and Katcoff, 1969; Friedlander et al., 1981). Molybdenum-99 is expected to be near the top of the yield-versus-mass curve on the light fraction side. As pointed out earlier, the cross-section for ^{99}Mo is ~35 mb, and remains constant with increasing proton energy. On the heavy fraction side of the yield-versus-mass curve and consistent with an earlier report (Hudis and Katcoff, 1969), cross-sections for ^{141}Ce, ^{143}Ce and ^{144}Ce all show decreasing trends with increasing proton energy. Cross sections for ^{139}Ce, however, show an increasing trend from 0.4 to 1.4 mb with increasing proton energy. At incident proton energies of 70 and 192 MeV, ^{139}Ce cross-sections are ~40 and ~5 times lower than the cross-sections for other Ce isotopes, respectively. As noted earlier, since ^{139}Ce is located on the neutron deficient side of β stability, it is likely not formed

from a fission process but rather through a fragmentation or spallation-like process (Friedlander et al., 1981).

4.4 Projected Yields

From the cross sections presented in this work, yields for the eleven radioisotopes were projected for beam currents and incident proton energies of 250 μA at 90 MeV for IPF and 100 μA at 191.8 MeV for BLIP for a continuous 10 day irradiation using a 5 g cm^{-2} Th target. These values are similar to those of the previous irradiations performed (Table 1). Table 5 outlines the calculated yields at EOB. Using the parameters described for IPF, the yield of ^{225}Ac is calculated to be 1.50 Ci with an ^{227}Ac/^{225}Ac ratio of 0.18%, while the total yield of all of the remaining radioisotopes reported here is 30.6 Ci. Using the BLIP irradiation parameters, the yield of ^{225}Ac is calculated to be 1.54 Ci with an ^{227}Ac/^{225}Ac ratio of 0.20%, and the total yield of the others reported is 13.0 Ci.

As indicated in Table 5 and discussed earlier, the projected yields of ^{225}Ac from the two irradiation facilities are very similar despite lower proton current at BLIP relative to IPF, reflecting the fact that the effective cross section for the ^{232}Th[p,x]^{225}Ac reaction increases with increasing incident proton energy from 78 to 191.8 MeV by a factor of about two (Figure 2). It appears the ratio of ^{227}Ac to ^{225}Ac also remains comparable in both facilities. The physical differences between the two irradiation facilities with regard to proton current and proton energy, however, are responsible for the apparent discrepancy between the projected yield of selected fission products and actinides — excluding ^{225}Ac (summarized in Table 5). The main factor responsible for this is the change in the shape of the corresponding excitation function as a function of energy. A number of additional actinides and hundreds of fission products were also detected over the course of these experiments, but reporting the yields of these additional nuclides is beyond the scope of this work, and will be reported in the future. Accurate quantification of these unreported isotopes, however, would require further chemical separations.

5. Conclusion and Future Work

Measured cross sections are reported here for eleven isotopes of Ac, Th, Mo, Ba/La, and Ce This data set validates previously reported measurements for many of these isotopes, and greatly expands the data available for other reaction cross sections such as that for ^{99}Mo. The

^{232}Th[p,f]^{144}Ce reaction cross section between 83 and 190 MeV is reported here for the first time. The data presented here will aid in the development of future irradiations of Th and subsequent chemical purifications of ^{225}Ac on a production scale for medical applications in targeted alpha radioimmunotherapy. As documented, curie quantities of ^{225}Ac can be produced in a ten-day irradiation of a 5 g cm^{-2} Th target at either LANL-IPF or BNL-BLIP. We will report the development of the related chemical processing and new target designs in future publications.

Acknowledgements

The authors acknowledge Drs. Tim S. Bigelow and Paul E. Mueller for their critical review of the manuscript. The authors thank the LANL Metallurgy group and the BNL machine shop teams for their efforts related to the fabrication of the targets used in this study. This research is supported by the Isotope Program, Office of Nuclear Physics of the U.S. Department of Energy. ORNL is managed by UT-Battelle, LLC, for the U.S. Department of Energy under contract DE-AC05-00OR22725.

References

Apostolidis, C., Molinet, R., McGinley, J., Abbas, K., Möllenbeck, J., and Morgenstern, A. (2005). Cyclotron production of Ac-225 for targeted alpha therapy. Applied Radiation and Isotopes *62*, 383-387.

Artna-Cohen, A. (1997). Nuclear Data Sheets for A = 224. Nuclear Data Sheets *80*, 227-262.

Basunia, M.S. (2007). Nuclear Data Sheets for A = 213. Nuclear Data Sheets *108*, 633-680.

Boll, R.A., Garland, M.A., and Mirzadeh, S. (2008). Production of Thorium-229 at the ORNL High Flux Isotope Reactor. Paper presented at: ANS Annual Meeting: Isotopes for Medicine and Industry (Anaheim, CA: ANS).

Boll, R.A., Malkemus, D., and Mirzadeh, S. (2005). Production of actinium-225 for alpha particle mediated radioimmunotherapy. Applied Radiation and Isotopes *62*, 667-679.

Brechbiel, M.W. (2007). Targeted α-therapy: past, present, future? Dalton Transactions, 4918-4928.

Browne, E. (2001). Nuclear Data Sheets for A = 215,219,223,227,231. Nuclear Data Sheets *93*, 763-1061.

Browne, E. (2005). Nuclear Data Sheets for A = 212. Nuclear Data Sheets *104*, 427-496.

Browne, E., and Tuli, J.K. (2011). Nuclear Data Sheets for A = 99. Nuclear Data Sheets *112*, 275-446.

Browne, E., and Tuli, J.K. (2012). Nuclear Data Sheets for A = 143. Nuclear Data Sheets *113*, 715-908.

Burrows, T.W. (2001). Nuclear Data Sheets for A = 139. Nuclear Data Sheets *92*, 623-782.

Canberra (2009). Genie 2000 Spectroscopy Software: Customization Tools.

de Kruijff, R., Wolterbeek, H., and Denkova, A. (2015). A Critical Review of Alpha Radionuclide Therapy—How to Deal with Recoiling Daughters? Pharmaceuticals *8*, 321.

Duijvestijn, M.C., Koning, A.J., Beijers, J.P.M., Ferrari, A., Gastal, M., van Klinken, J., and Ostendorf, R.W. (1999). Proton-induced fission at 190 MeV of ^{nat}W, ^{197}Au, ^{nat}Pb, ^{208}Pb, and ^{232}Th. Physical Review C *59*, 776-788.

Engle, J.W., Weidner, J.W., Ballard, B.D., Fassbender, M.E., Hudston, L.A., Jackman, K.R., Dry, D.E., Wolfsberg, L.E., Bitteker, L.J., and Ullmann, J.L. (2014). Ac, La, and Ce radioimpurities in ^{225}Ac produced in 40–200 MeV proton irradiations of thorium. Radiochimica Acta *102*, 569-581.

Ermolaev, S.V., Zhuikov, B.L., Kokhanyuk, V.M., Matushko, V.L., Kalmykov Stepan, N., Aliev Ramiz, A., Tananaev Ivan, G., and Myasoedov Boris, F. (2012). Production of actinium, thorium and radium isotopes from natural thorium irradiated with protons up to 141 MeV. Radiochimica Acta *100*, 223.

Essler, M., Gärtner, F.C., Neff, F., Blechert, B., Senekowitsch-Schmidtke, R., Bruchertseifer, F., Morgenstern, A., and Seidl, C. (2012). Therapeutic efficacy and toxicity of ^{225}Ac-labelled vs. ^{213}Bi-labelled tumour-homing peptides in a preclinical mouse model of peritoneal carcinomatosis. European Journal of Nuclear Medicine and Molecular Imaging *39*, 602-612.

Friedlander, G., Kennedy, J.W., Macias, E.S., and Miller, J.M. (1981). Nuclear and Radiochemistry, 3rd edn (New York: John Wiley & Sons, Inc.).

Gauvin, H. (1963). Reactions (p, 2pxn) sur le thorium 232 de 30 à 120 MeV. J Phys France *24*, 836-838.

Hogan, J.J., Gadioli, E., Gadioli-Erba, E., and Chung, C. (1979). Fissionability of nuclides in the thorium region at excitation energies to 100 MeV. Physical Review C *20*, 1831-1843.

Holub, R., and Yaffe, L. (1973). Charge dispersion studies of heavy-mass elements in the fission of ^{232}Th by protons of medium energy. Journal of Inorganic and Nuclear Chemistry *35*, 3991-4000.

Hudis, J., and Katcoff, S. (1969). High-Energy-Proton Fission Cross Sections of U, Bi, Au, and Ag Measured with Mica Track Detectors. Physical Review *180*, 1122-1130.

IAEA (2013). Technical Meeting on Alpha emitting radionuclides and radiopharmaceuticals for therapy.

Jost, C.U., Griswold, J.R., Bruffey, S.H., Mirzadeh, S., Stracener, D.W., and Williams, C.L. (2013). Measurement of cross sections for the ^{232}Th(p,4n)^{229}Pa reaction at low proton energies. AIP Conference Proceedings: International Conference on Application of Accelerators in Research and Industry, *1525*, 520-524.

Jurcic, J.G., and Rosenblat, T.L. (2014). Targeted alpha-particle immunotherapy for acute myeloid leukemia. Am Soc Clin Oncol Educ Book, e126-131.

Kumar Jain, A., Singh, S., Kumar, S., and Tuli, J.K. (2007). Nuclear Data Sheets for A = 221. Nuclear Data Sheets *108*, 883-922.

Lefort, M., Simonoff, G.N., and Tarrago, X. (1961). Spallation Reactions of Thorium by 150 and 82 MeV Protons. Nuclear Physics *25*, 216-247.

Lisowski, P.W., and Schoenberg, K.F. (2006). The Los Alamos Neutron Science Center. Nuclear Instruments and Methods in Physics Research Section A: Accelerators, Spectrometers, Detectors and Associated Equipment *562*, 910-914.

McDevitt, M.R., Ma, D., Lai, L.T., Simon, J., Borchardt, P., Frank, R.K., Wu, K., Pellegrini, V., Curcio, M.J., Miederer, M., *et al.* (2001). Tumor Therapy with Targeted Atomic Nanogenerators. Science *294*, 1537-1540.

McLaughlin, M.F., Woodward, J.D., Boll, R.A., Wall, J.S., Rondinone, A.J., Kennel, S.J., Mirzadeh, S., and Robertson, J.D. (2013). Gold Coated Lanthanide Phosphate Nanoparticles for Targeted Alpha Generator Radiotherapy. PLOS One.

Medvedev, D.G., Mausner, L.F., Meinken, G.E., Kurczak, S.O., Schnakenberg, H., Dodge, C.J., Korach, E.M., and Srivastava, S.C. (2012). Development of a large scale production of ^{67}Cu from ^{68}Zn at the high energy proton accelerator: Closing the ^{68}Zn cycle. Applied Radiation and Isotopes *70*, 423-429.

Melville, G., Meriarty, H., Metcalfe, P., Knittel, T., and Allen, B.J. (2007). Production of Ac-225 for cancer therapy by photon-induced transmutation of Ra-226. Applied Radiation and Isotopes *65*, 1014-1022.

Mirzadeh, S. (1998). Generator-produced alpha-emitters. Applied Radiation and Isotopes *49*, 345-349.

Mirzadeh, S. (2014). Accelerator produced ^{225}Ac via proton spallation of ^{232}Th: a joint research program among ORNL, LANL, and BNL. ORNL report TM-2014-142, Oak Ridge, USA.

Mulvey, J.J., Villa, C.H., McDevitt, M.R., Escorcia, F.E., Casey, E., and Scheinberg, D.A. (2013). Self-assembly of carbon nanotubes and antibodies on tumours for targeted amplified delivery. Nat Nano *8*, 763-771.

Nica, N. (2007). Nuclear Data Sheets for A = 140. Nuclear Data Sheets *108*, 1287-1470.

Nica, N. (2014). Nuclear Data Sheets for A = 141. Nuclear Data Sheets *122*, 1-204.

Radchenko, V., Engle, J.W., Wilson, J.J., Maassen, J.R., Nortier, F.M., Taylor, W.A., Birnbaum, E.R., Hudston, L.A., John, K.D., and Fassbender, M.E. (2015). Application of ion exchange and

extraction chromatography to the separation of actinium from proton-irradiated thorium metal for analytical purposes. Journal of Chromatography A *1380*, 55-63.

Raparia, D., Briscoe, B., Cerniglia, P., Connolly, R., Cullen, C., Gassner, D., Hulsart, R., Lambliase, R., LoDestro, V., and Mausner, L. (2014). Uniform Current Density for BLIP Target at Brookhaven 200 MeV LINAC. Paper presented at: LINAC2014 (Geneva, Switzerland).

Rojas, J.V., Woodward, J.D., Chen, N., Rondinone, A.J., Castano, C.H., and Mirzadeh, S. (2015). Synthesis and characterization of lanthanum phosphate nanoparticles as carriers for ^{223}Ra and ^{225}Ra for targeted alpha therapy. Nuclear Medicine and Biology *42*, 614-620.

Singh, S., Jain, A.K., and Tuli, J.K. (2011). Nuclear Data Sheets for A = 222. Nuclear Data Sheets *112*, 2851-2886.

Sonzogni, A.A. (2001). Nuclear Data Sheets for A = 144. Nuclear Data Sheets *93*, 599-762.

Steyn, G.F., Mills, S.J., Nortier, F.M., Simpson, B.R.S., and Meyer, B.R. (1990). Production of ^{52}Fe Via Proton-Induced Reactions on Manganese and Nickel. Applied Radiation and Isotopes *41*, 315-325.

Titarenko, Y.E., Batyaev, V., and Karpikhin, E. (2003). Experimental and theoretical study of the yields of residual product nuclei produced in thin targets irradiated by 100-2600 MeV protons (International Nuclear Data Committee).

Weidner, J.W., Mashnik, S.G., John, K.D., Hemez, F., Ballard, B., Bach, H., Birnbaum, E.R., Bitteker, L.J., Couture, A., Dry, D., *et al.* (2012). Proton-induced cross sections relevant to production of ^{225}Ac and ^{223}Ra in natural thorium targets below 200 MeV. Applied Radiation and Isotopes *70*, 2602-2607.

Zhuikov, B.L., Kalmykov, S.N., Ermolaev, S.V., Aliev, R.A., Kokhanyuk, V.M., Matushko, V.L., Tananaev, I.G., and Myasoedov, B.F. (2011). Production of ^{225}Ac and ^{223}Ra by irradiation of Th with accelerated protons. Radiochemistry *53*, 73-80.

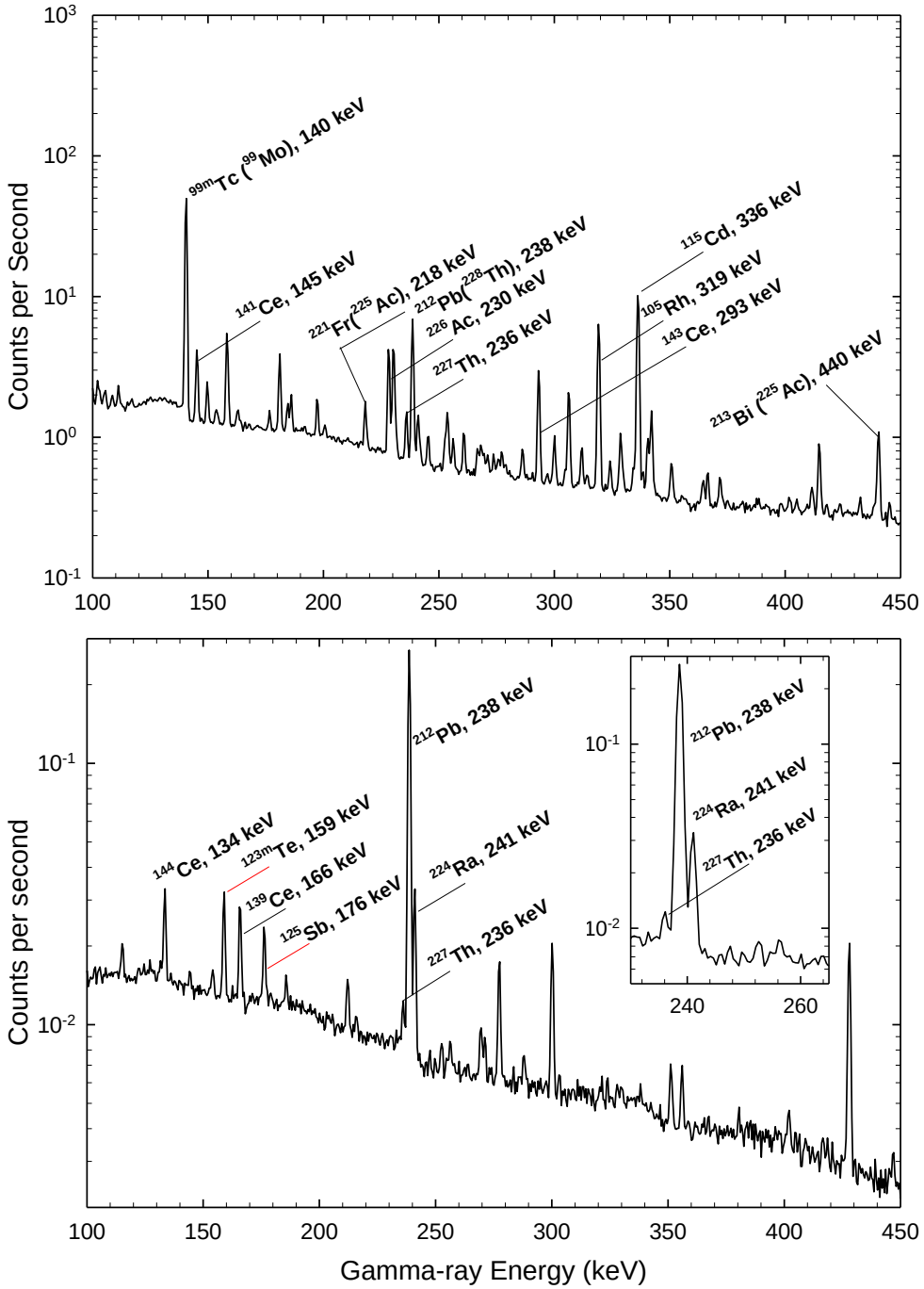

Figure 1. Gamma-ray spectra of a sample of target solution taken ~57 hours post EOB (TOP), and after ~17 months of decay (BOTTOM). As indicated in the expanded view, the 236 keV γ-ray peak from ^{227}Th ($t_{1/2}$ = 18.7 d) is visible after 16 months of decay — an indication of presence of the ^{227}Ac ($t_{1/2}$ = 21.8 y) predecessor in the sample.

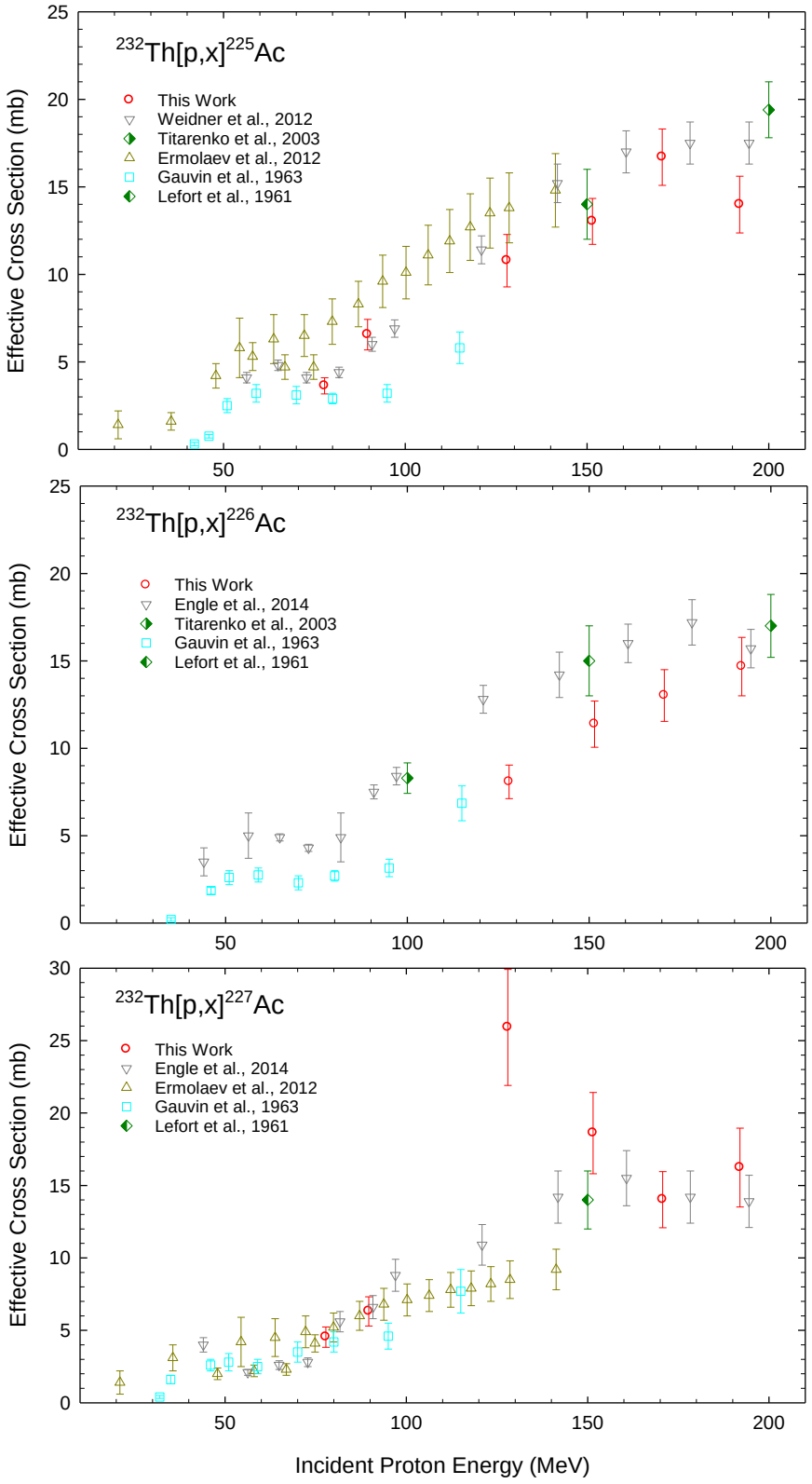

Figure 2. Measured effective cross sections for the ^{232}Th[p,x]^{225,226,227}Ac reactions from 20-200 MeV.

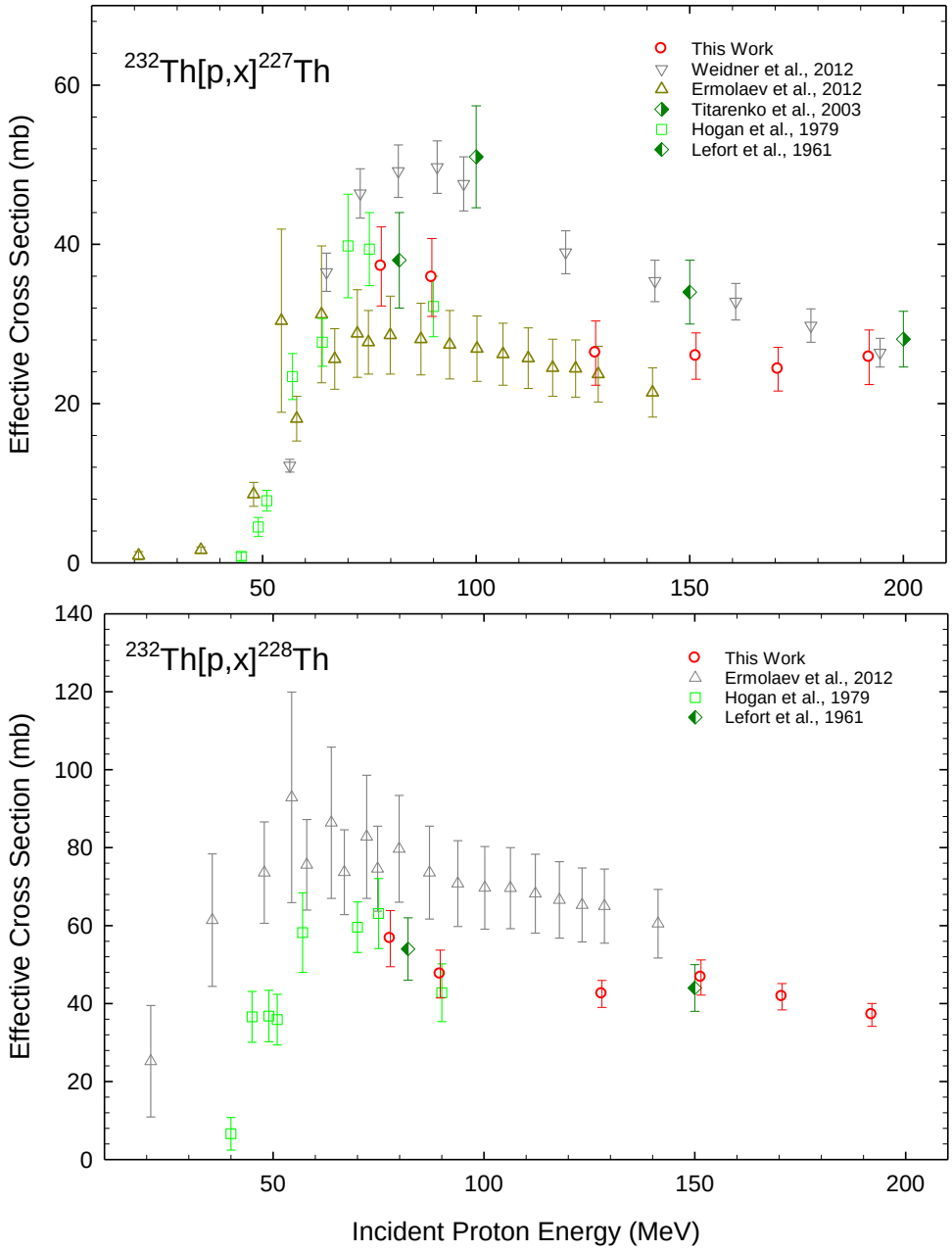

Figure 3. Measured effective cross sections for the ^{232}Th[p,x]^{227,228}Th reactions from 20-200 MeV.

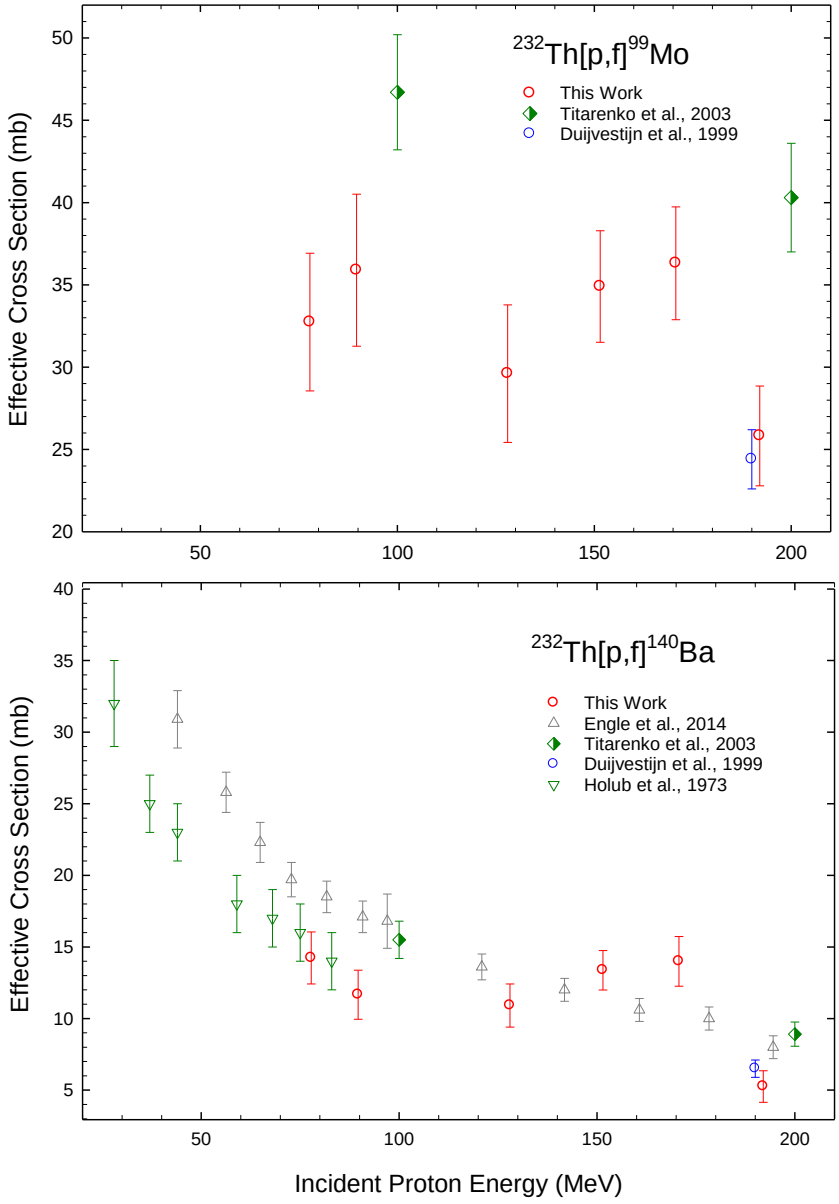

Figure 4. Measured effective cross sections for the ^{232}Th[p,f]^{99}Mo reaction and the ^{232}Th[p,f]^{140}Ba reaction from 20-200 MeV.

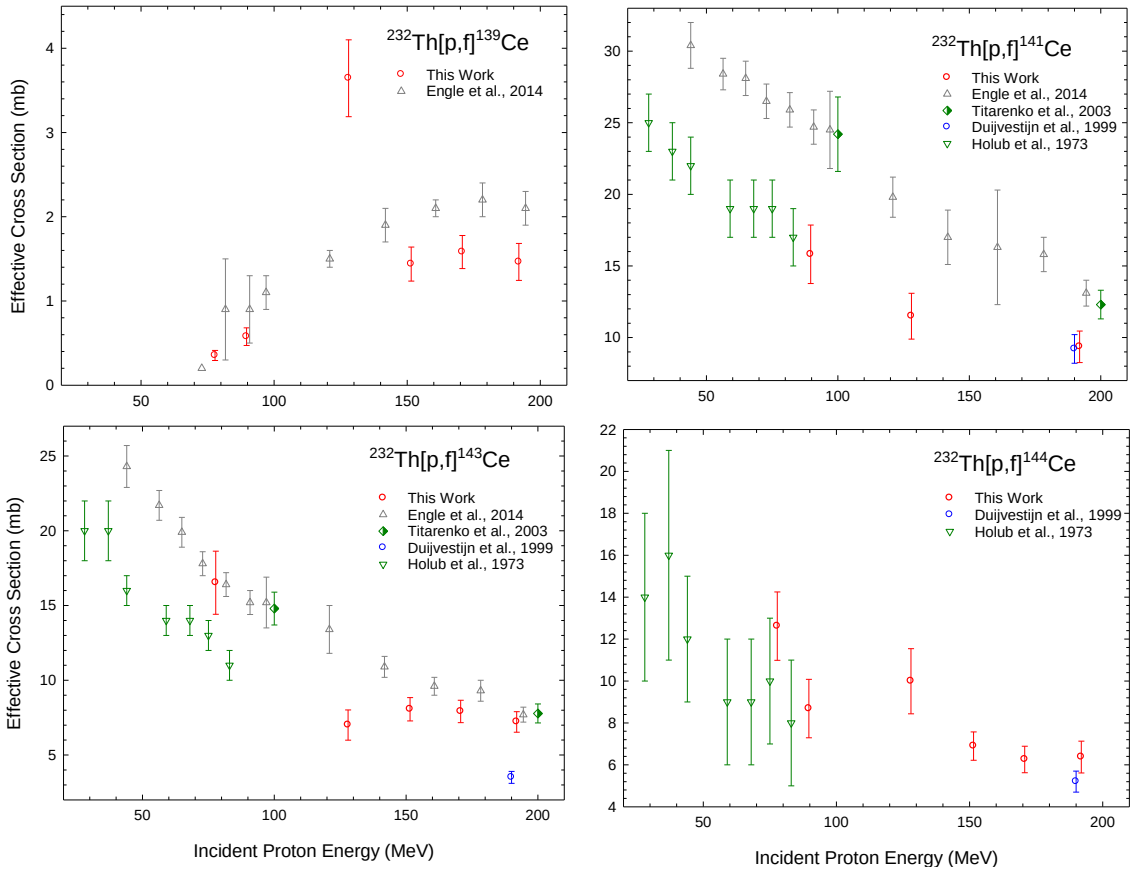

Figure 5. Measured effective cross sections for the ^{232}Th[p,f]^{139,141,143,144}Ce reactions from 20-200 MeV.

Table 1. Irradiation Parameters

Number	Target Thickness (mg cm^{-2})	Incident Energy (MeV)	Exit Energy (MeV)	Irradiation Period (h)	Average Current (μA)
Irradiations at IPF					
1	637.6	77.4	74.8	24.2	207.1
2	634.6	89.6	87.2	24.1	208.3
3	634.6	89.6	87.2	91.5	159.5
Irradiations at BLIP					
4	166.0	128.1	127.6	3.6	87.2
5	519.5	129.6	128.2	17.0	54.1
6	157.4	128.1	127.6	107.4	45.1
*7a	164.5	128.1	127.6	137.6	36.6
*7b	168.5	128.1	127.6	137.6	36.6
8	366.3	129.6	128.7	190.3	50.8
9	146.3	128.1	127.6	16.0	23.6
10	146.3	152.7	152.3	16.0	30.7
11	146.3	173.8	173.5	16.0	29.9
12	592.8	192.3	190.8	218.2	108.5
13	579.2	192.3	190.8	222.0	116.4
14	438.8	192.4	191.3	215.3	93.1
15	146.3	192.3	191.9	16.8	65.2
16	527.2	192.3	191.0	191.4	86.0

*Targets 7a and 7b consisted of two Th foils that were irradiated together but processed separately.

Table 2. Principal γ-ray emissions used for assay of radionuclides in this work.

Radionuclide	Half-life	Eγ (keV)	Iγ (%)	Cool-Off Period Required?	Reaction Pathways	Comments
^{99}Mo	66.0 h	739.5	12.3	No	^{232}Th[p,f]	
^{140}Ba	12.8 d	537.3	24.4	No	^{232}Th[p,f]	
^{139}Ce	137.6 d	165.9	80.0	Yes	^{232}Th[p,f]	
^{141}Ce	32.5 d	145.4	48.3	Yes	^{232}Th[p,f]	
^{143}Ce	33.0 h	293.3	42.8	No	^{232}Th[p,f]	
^{144}Ce	284.9 d	133.5	11.1	Yes	^{232}Th[p,f]	
^{225}Ac	9.92 d	440.5 (^{213}Bi)	25.9	No	^{232}Th[p,α4n]^{225}Ac ^{232}Th[p,αp3n]^{225}Ra[β-,14.9d]→^{225}Ac ^{232}Th[p,p7n]^{225}Th[EC, 8.8m]→^{225}Ac	Assayed from ^{213}Bi daughter
^{226}Ac	29.4 h	230.0	26.9	No	^{232}Th[p,α3n]^{226}Ac	
^{227}Ac	21.8 y	236.0 (^{227}Th)	12.9	Yes	^{232}Th[p,α2n]^{227}Ac ^{232}Th[p,αpn]^{227}Ra(β-,42.2m)→^{227}Ac	See text for assay method.
^{227}Th	18.7 d	236.0	12.9	No	^{232}Th[p,p5n]^{227}Th ^{232}Th[p,6n]^{227}Pa(EC,38.3m)→^{227}Th	Also used to quantify ^{227}Ac after Th separation and decay
^{228}Th	1.91 y	238.6 (^{212}Pb)	43.6	Yes	^{232}Th[p,p4n]^{228}Th ^{232}Th[p,5n]^{228}Pa(EC,22.4h)→^{228}Th ^{232}Th[p,αn]^{228}Ac(β^-,6.2h)→^{228}Th	Assayed from ^{212}Pb daughter

Table 3. Effective production cross sections of ^{225}Ac and other radioisotopes from ^{232}Th target irradiated with 78-90 MeV protons at IPF.

Isotope	Half-life	Effective Cross Section (mb) at	
		77.8 ± 0.4 MeV	89.6 ± 0.4 MeV
^{225}Ac	9.92 d	3.6 ± 0.5	6.6 ± 0.9
^{226}Ac	29.37 h	N/M	N/M
^{227}Ac	21.77 y	4.5 ± 0.7	6.3 ± 1.0
^{227}Th	18.72 d	37.2 ± 5.0	35.8 ± 4.9
^{228}Th	697.15 d	56.7 ± 7.2	47.6 ± 6.1
^{99}Mo	65.98 h	32.7 ± 4.2	35.9 ± 4.6
^{140}Ba	12.75 d	14.2 ± 1.8	11.7 ± 1.7
^{139}Ce	137.64 d	0.4 ± 0.1	0.6 ± 0.1
^{141}Ce	32.50 d	N/M	15.8 ± 2.0
^{143}Ce	33.04 h	16.5 ± 2.1	N/M
^{144}Ce	285.00 d	12.6 ± 1.6	8.7 ± 1.4

*N/M = Not measured

Table 4. Effective production cross sections of ^{225}Ac and other radioisotopes from ^{232}Th target irradiated with 128-192 MeV protons at BLIP.

Isotope	Half-life	Effective Cross Section (mb) at 128.0 ± 0.4 (MeV)	151.5 ± 0.4 (MeV)	170.7 ± 0.4 (MeV)	191.8 ± 0.4 (MeV)
^{225}Ac	9.92d	10.8 ± 1.5	13.0 ± 1.3	16.7 ± 1.6	14.0 ± 1.6
^{226}Ac	29.37h	8.1 ± 1.0	11.4 ± 1.3	13.0 ± 1.5	14.7 ± 1.7
^{227}Ac	21.77y	26.5 ± 3.5	18.6 ± 2.8	14.0 ± 1.9	16.2 ± 2.7
^{227}Th	18.72d	26.3 ± 4.0	26.0 ± 2.9	24.3 ± 2.7	25.8 ± 3.4
^{228}Th	697.15d	42.5 ± 4.0	46.7 ± 4.5	41.8 ± 3.9	37.1 ± 3.1
^{99}Mo	65.98h	29.6 ± 4.2	34.9 ± 3.4	36.3 ± 3.4	25.8 ± 3.0
^{140}Ba	12.75d	10.9 ± 1.5	13.4 ± 1.4	14.0 ± 1.7	5.2 ± 1.1
^{139}Ce	137.64d	3.6 ± 0.5	1.4 ± 0.2	1.6 ± 0.2	1.5 ± 0.2
^{141}Ce	32.50d	11.5 ± 1.6	N/M	N/M	9.4 ± 1.1
^{143}Ce	33.04h	7.0 ± 1.0	8.1 ± 0.8	7.9 ± 0.7	7.2 ± 0.7
^{144}Ce	285.00d	10.0 ± 1.5	6.9 ± 0.7	6.3 ± 0.6	6.4 ± 0.8

*N/M = Not measured

Table 5. Yield calculations (at EOB) for radionuclides reported in this text, based on a 10 day irradiation of a 5 g cm^{-2} Th target.

	IPF Yield (250μA, 90 MeV)		**BLIP Yield (100μA, 192 MeV)**	
Radionuclide	**(Ci)**	**(GBq)**	**(Ci)**	**(GBq)**
^{225}Ac	1.5	55.6	1.5	57.1
^{226}Ac	N/M	N/M	3.2	118.6
^{227}Ac	2.7×10^{-3}	0.1	3.1×10^{-3}	0.1
^{227}Th	6.3	232.3	1.9	70.4
^{228}Th	0.2	8.1	0.1	2.8
^{99}Mo	18.1	669.1	5.4	199.9
^{140}Ba	3.1	116.1	0.5	16.9
^{139}Ce	1.1×10^{-2}	0.4	1.6×10^{-2}	0.6
^{141}Ce	1.4	52.5	0.4	13.1
^{143}Ce	1.4	51.1	1.6	58.1
^{144}Ce	0.1	3.5	3.3×10^{-2}	1.2

*N/M = Not measured

Supplemental Material

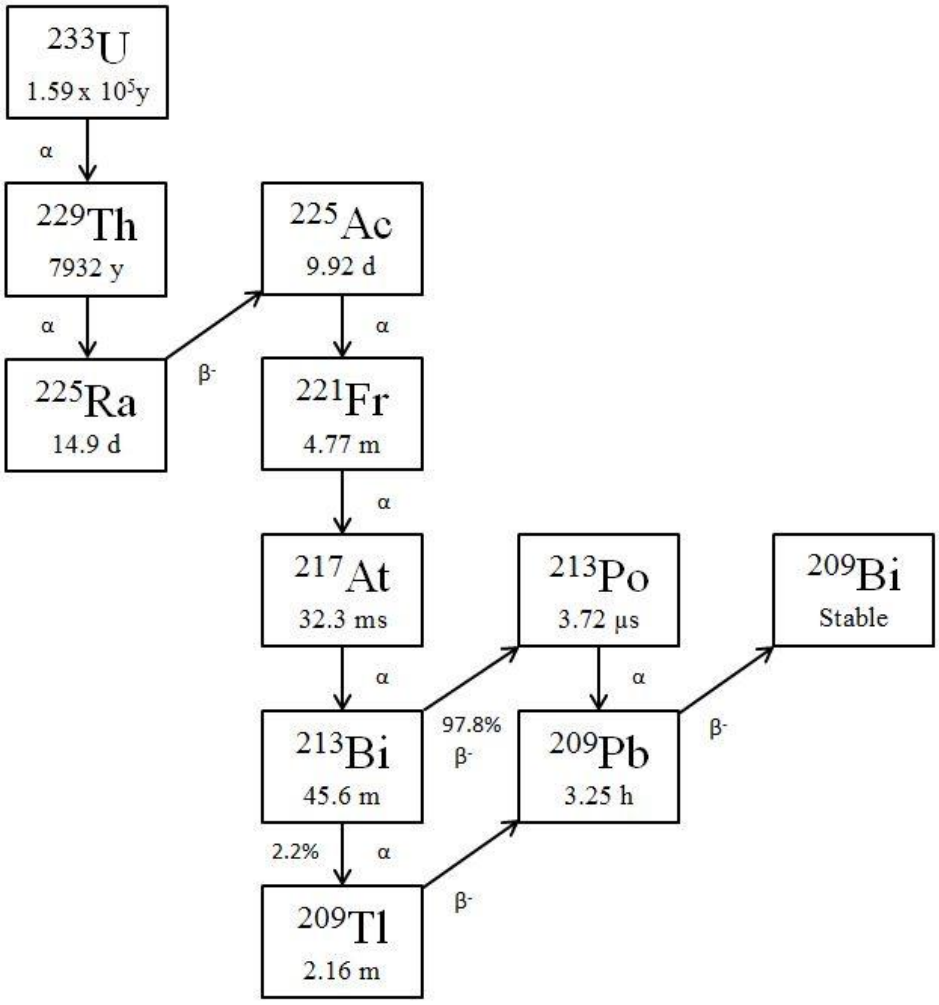

Figure S1. Uranium-233 Decay Chain.

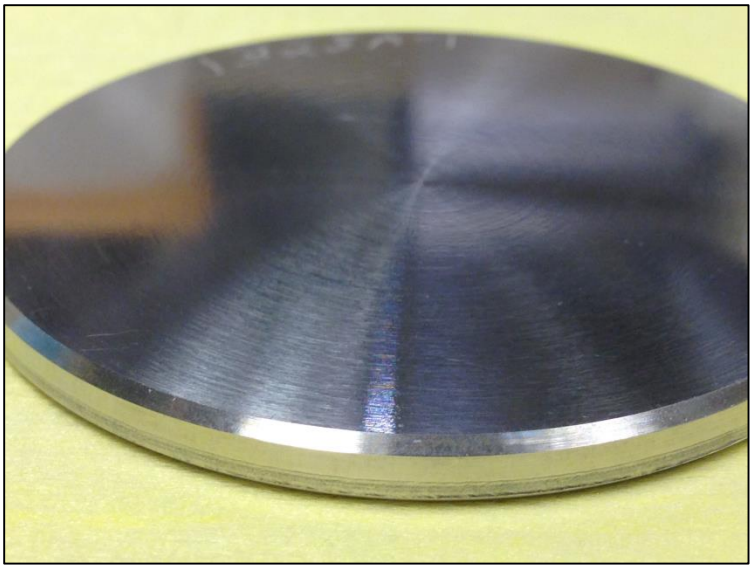

Figure S2. Inconel-encapsulated Th disk before irradiation at IPF.

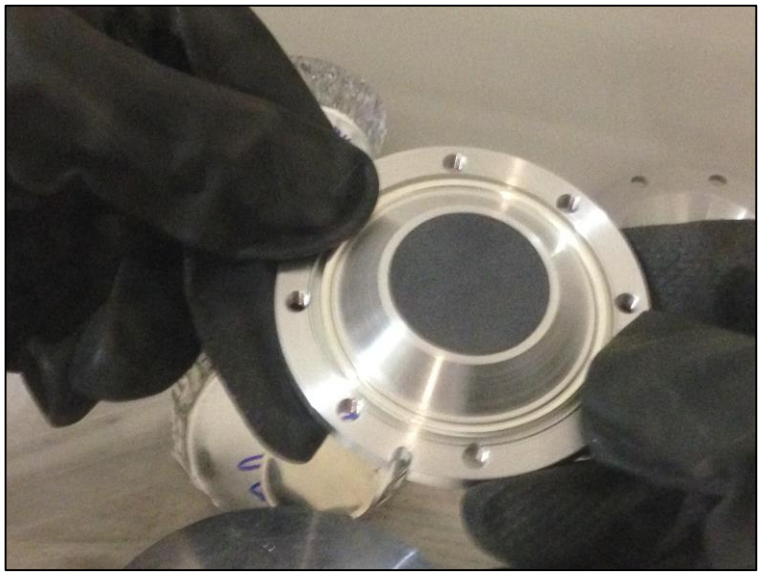

Figure S3. Aluminum target holder with Th disk before irradiation at BLIP.